Electrical and Computer Engineering Faculty
Research & Creative Works

Electrical and Computer Engineering

01 Jul 2014

# Integration of Microwave and Thermographic NDT Methods for Corrosion Detection

Dustin F. Pieper

Kristen M. Donnell
*Missouri University of Science and Technology*, kmdgfd@mst.edu

Mohammad Tayeb Ahmad Ghasr
*Missouri University of Science and Technology*, mtg7w6@mst.edu

Edward C. Kinzel
*Missouri University of Science and Technology*, kinzele@mst.edu

Follow this and additional works at: https://scholarsmine.mst.edu/ele_comeng_facwork

 Part of the Electrical and Computer Engineering Commons, and the Mechanical Engineering Commons

# Integration of Microwave and Thermographic NDT Methods for Corrosion Detection

D. Pieper[a], K.M. Donnell[a], M.T. Ghasr[a] and E.C. Kinzel[b]

[a]Applied Microwave Nondestructive Testing Laboratory (amntl), Department of Electrical and Computer Engineering
[b]Department of Mechanical and Aerospace Engineering
[a,b]Missouri University of Science and Technology, 301 W. 16th St, Rolla, MO 65409

**Abstract.** Infrastructure health monitoring is an important issue in the transportation industry. For the case of cement-based structures in particular, detection of corrosion on reinforcing steel bars (rebar) is an ongoing problem for aging infrastructure. There have been a number of techniques that have shown promise in this area including microwave nondestructive testing (NDT) and thermography. Thermography is quite advantageous as it is an established method, and can be utilized for large inspection areas with intuitive results. Typical heat sources include induction heating and flash lamps, but these are not without drawbacks. Microwave nondestructive testing has also been successful at detecting corroded rebar, but at the cost of lengthy scan times. This paper presents an investigation into the potential of utilizing aspects of microwave NDT and thermography to create a hybrid NDT method, herein referred to as Active Microwave Thermography (AMT). AMT takes advantage of the electromagnetically lossy nature of corrosion byproducts and uses microwave energy to induce heat in the corrosion. Subsequently, the resultant heat profile is captured using an infrared camera. This paper presents initial simulations and measurements that highlight the potential of AMT to detect corroded rebar.

**Keywords:** Microwave Nondestructive Testing, Thermography, Corrosion Detection, Reinforcing Steel Bars, Hybrid NDT Methodology.
**PACS:** 84.40.-x, 87.63.Hg, 81.70.-q,

## INTRODUCTION

Health monitoring of infrastructure is an important ongoing concern in the transportation industry. In particular for cement-based infrastructure, detection and characterization of corroded reinforcing steel bars (rebar) is of interest. According to United States Department of Transportation (USDOT), the direct cost of corrosion on highway bridges is estimated at $8.3 billion [1]. Current methods for detecting corrosion on rebar are primarily electrochemical-based techniques, which are not truly nondestructive [2]. Many nondestructive testing (NDT) techniques have been studied for this purpose, including ultrasound, microwave NDT, thermography, etc. [3-6]. Thermography is a well-established NDT technique, and has been successfully applied in many areas including crack detection in metals, stress analysis, and fatigue damage in composite materials [7-9]. Thermography is a powerful NDT method, with benefits including high accuracy, fast response times over large inspection areas, and intuitive results. Moreover, modern infrared cameras allow rapid, non-contact measurement of the surface temperature of a sample under test (SUT). NDT applications of thermography involve detecting and identifying discontinuities by observing their effect on the real-time surface temperature as heat diffuses through the SUT. Active thermography utilizes an external heat source such as a flash lamp, or through eddy current (induction) heating [10]. These heating techniques have limitations; for example, eddy current heating is limited to conductive materials (useful if heating of a rebar itself is desired, but not for heating a dielectric such as corrosion) and flash lamp heating suffers from long thermal propagation times, in addition to risking heat damage.

Microwave materials characterization has shown success for determining important characteristics of cement-based materials including cure state monitoring and determination of water-to-cement ratio (*w/c*), sand-to-cement ratio (*s/c*), coarse aggregate-to-cement ratio (*ca/c*) [11], coarse aggregate content distribution and segregation [12, 13], as well as chloride ingress in mortar [14, 15]. Similarly, microwave imaging has shown promise for detecting the presence of corrosion [6], but at the cost of lengthy evaluation time. Thermographic methods have also shown promise for cement-based infrastructure inspection, including crack detection [16].

This paper demonstrates the potential of utilizing aspects of microwave NDT and thermography to create a hybrid NDT method, herein referred to as Active Microwave Thermography (AMT), and the capability of the technique to detect corroded rebar. Specifically, the feasibility of utilizing microwave energy to locally heat corrosion on steel reinforcing bars in concrete structures is presented. Steel corrosion byproducts are electromagnetically lossy and can be easily heated using microwave energy. Subsequently, the heat profile is mapped using an IR camera. Utilizing microwave energy is advantageous since microwave energy can penetrate concrete and locally heat the area of interest.

## SIMULATIONS

In order to study the interaction between an electromagnetic signal and induced heating, a coupled microwave and thermal simulation model was constructed using the CST MICROWAVE STUDIO® and MPHYSICS STUDIO®. This model allowed the electromagnetic (specifically, polarization of the incident signal) and thermal properties exhibited by corroded rebar surrounded by air under planewave incidence to be studied. First, the thermal response resulting from microwave heating was simulated for an infinitely-long rebar as a function of (uniform) corrosion thickness. A second simulation was conducted to study the electromagnetic and thermal properties of a finite-length rebar with an area of corrosion. Lastly, a third CST simulation was developed that examined the thermal response of two finite lengths of rebar, one fully corroded and one clean (i.e., without corrosion), embedded in a concrete block. In all cases, a frequency of 2.45 GHz (in the ISM band) was selected for the incident microwave energy. This frequency was selected due to previous success with frequencies in the range for cement-based materials characterization, as well as for subsequent comparisons to measurements (which were conducted at a frequency of 2.45 GHz as well).

### Simulation of Rebar in Air

To begin studying the relationship between microwave heating and corrosion, an infinitely-long rebar of radius 4.8 mm with uniform corrosion on its surface was simulated. While an infinitely-long rebar will not be found in practice, studying such an element removes effects that may result from the geometry (i.e., finite rebar length) of a more practical model. For this model, the corrosion replaced part of the volume of the rebar (so as to properly reflect the corrosion process), meaning the radius of the steel core of the corroded rebar decreased as corrosion thickness increased. Specifically, the radius of the rebar decreased by 50% of the corrosion thickness. The rebar was assumed to be made of steel (AISI 1008). The corrosion had a relative permittivity, $\varepsilon_r = 10$ and loss tangent, $\tan \delta = 0.2$ (a typical value for steel corrosion [17]), thermal conductivity, $k_t = 0.6$ W/m·K, specific heat, $c_p = 650.6$ J/kg·K, and density $\rho = 5242$ kg/m$^3$ [18, 19]. The background material was assumed to be air ($\varepsilon_r = 1$, electrical conductivity, $\sigma = 0$ S/m, $k_t = 0.024$W/m·K, $c_p = 1005$ J/kg·K, and $\rho = 1.293$ kg/m$^3$). The magnitude of the incident electric field of the planewave was chosen to be $E_0 = 2500$ V/m, in order to simulate a $P = 50$W source being emitted from an R-band (1.7 – 2.6 GHz) waveguide aperture. This value was calculated using Eq. (1), below, where $E_0$ is incident electric field strength, $\eta$ is the impedance of the material in which the planewave is propagating (377 Ω for free-space), $P$ is the total power, and $A$ is the aperture of the radiating antenna (i.e. cross-section of the waveguide).

$$E_0 = \left( 2\eta \frac{P}{A} \right)^{1/2} \tag{1}$$

Using the model for an infinitely-long rebar, the effect of polarization on the thermal response of the rebar was investigated as a function of corrosion thickness. To this end, signals with polarization orthogonal and parallel to the length of the rebar were considered. In addition, the response from a circularly-polarization signal was also studied. From these excitations, the resultant (electromagnetically-induced) thermal losses and subsequent maximum temperature increase of the rebar were calculated. The maximum temperature difference (as compared to the initial/ambient temperature of the rebar) for the three different polarizations as a function of corrosion thickness can be found below in Fig. 1.
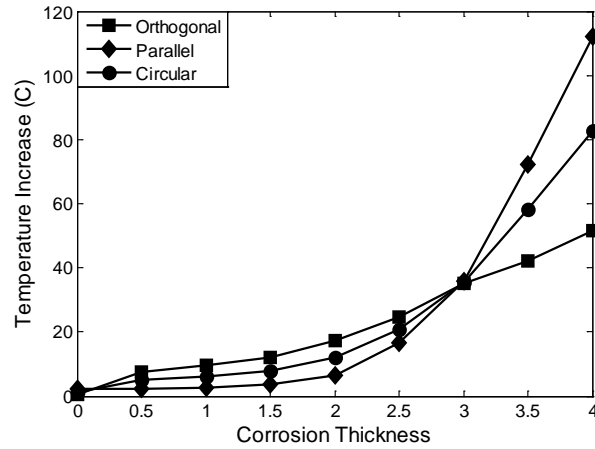
**FIGURE 1.** Max temperature of corroded rebar for different polarizations over different corrosion thickness cases.

As mentioned above, corrosion by-products are electromagnetically lossy. As such, it is expected that as the thickness of corrosion increases, so should the microwave-induced heating. This behavior is evident in Fig. 1 for all three polarizations. It can also be seen that as the thickness of corrosion increases, the temperature increase due to the parallel-polarized signal follows an exponential curve, while the effect of orthogonal polarization is linear. Furthermore, for corrosion of less than 3 mm, orthogonal polarization is optimal, while for significant corrosion (> 3 mm), parallel becomes best. This is important since, depending on the severity of corrosion, the polarization can be optimized to achieve maximum heating (if the orientation of the rebar is known). It can also be seen that the induced heat from circular polarization is the average of the heating from parallel and perpendicular polarization. While circular polarization does not result in the maximum induced heat, it does offer an independence from rebar orientation (with respect to the polarization of the incident signal), as well as an independence with respect to corrosion thickness. This is important since knowledge of the orientation of the rebar may not be available in practice. However, utilizing circular polarization will be at the expense of a more sophisticated microwave antenna and/or measurement system.

Once the effect of polarization was understood, a finite-length rebar (in this case, 10 cm), a portion of which is corroded, was simulated, as is shown below in Fig. 2a. In this case, a 0.1 mm layer of corrosion was considered (length of the corroded section is 2 cm). The material properties for the steel rebar and corrosion remain as above. In this case, the magnitude of the incident electric field was chosen to be 500V/m (calculated using Eq. (1)), in order to simulate a 10 W source incident on an area of 17 cm × 15 cm (a relatively small footprint for inspection, utilizing fairly low power). All three polarizations were considered as well with the results shown below in Fig. 2b-d.
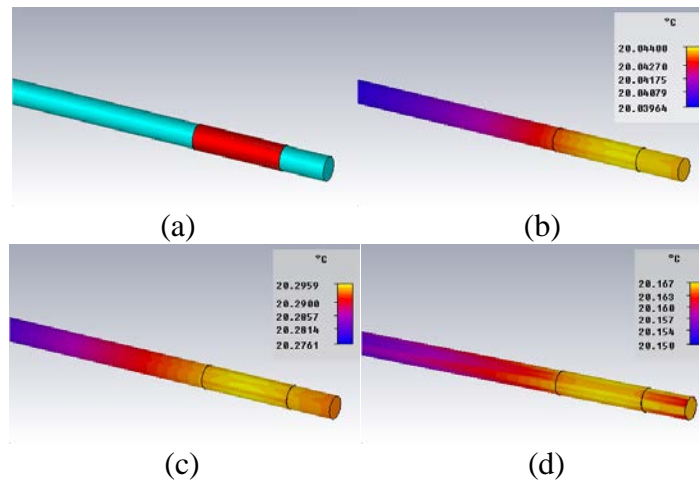


**FIGURE 2.** (a) Simulated rebar with corroded section. Heat distribution caused by (b) orthogonal polarization, (c) parallel polarization, and (d) circular polarization.

Fig. 2 shows that the polarization of the incident signal does not affect the heat distribution on the rebar. However, as in case of the infinitely-long rebar, more significant heating was evident in the corroded region as compared to the non-corroded region of the rebar. Furthermore, parallel polarization was found to cause the most heating, providing a temperature increase of 20° mC. The temperature increase for circular polarization was 17° mC, and for orthogonal polarization, 5° mC. While the increase in temperature simulated here is fairly small, this is not of concern, as the incident power considered is quite low (10 W), and the sensitivity of modern IR cameras is on the order of 50° mC or less. As such, with a reasonable increase in incident power, the change in temperature would be within a detectable range.

It is important to note that these results differ from those in Fig. 1, as according to Fig. 1, orthogonal polarization is best for thin corrosion. The results of Fig. 1 are for a completely-corroded infinitely-long rebar (allowing for a study of the sole effect of polarization), whereas Fig. 2 highlights results of a partially-corroded finite-length rebar where the geometry of the rebar (e.g., finite length/edge effects) may affect the results.

## Simulation of Rebar Embedded in Concrete

In order to investigate a more practical scenario, a simulation was conducted to model an embedded case. More specifically, two steel (AISI 1008) rebar sections (each of length 15 cm and radius 4.8 mm), one fully corroded and one uncorroded, were embedded (parallel to one another) in a concrete block (17 cm × 15 cm × 5cm). The rebars were placed a distance of ~4 cm apart. The rebars were located ~1.6 cm from the bottom of the block, and ~3 cm from the top. The corrosion was assumed to have the same electromagnetic and thermal properties as provided above. The concrete was assumed to have $\varepsilon_r = 5$, $k_t = 1.73$ W/m·K, $c_p = 800$ J/kg·K, and $\rho = 2400$ kg/m$^3$. A 10 W electromagnetic source operating at 2.45 GHz was assumed (as above).

To begin, the effect of polarization was studied. The CST model and heat distribution of the shallow side of the block for orthogonal, parallel, and circular polarization are shown in Fig. 3. The corroded bar (corrosion thickness 1 mm) is on the left. It can be observed that although parallel polarization (14° mC, Fig. 3c) creates less heating than orthogonal polarization (25° mC, Fig. 3b), the heat generated is more uniform along the length of the surface above the corroded rebar. Additionally, the temperature increase generated by circular polarization (19° mC, Fig. 3d) is approximately the average of parallel and perpendicular polarizations and also exhibits slightly less uniform heating over the length of the rebar. It is interesting to note that the results of Fig. 3 corroborate those of Fig. 1. Since the embedded concrete model considers a fully-corroded rebar, it is more similar to the infinitely-long model. As such, it is not unexpected that the results shown here may be similar to those of Fig. 1.

Next, simulations were conducted to investigate the effect of the loss tangent of the concrete on the induced heat. In practice, a concrete structure may be subject to moisture ingress, which would affect the electromagnetic properties of the concrete resulting in an increase in loss tangent. As the loss tangent of the surrounding material increases, more of the microwave energy may be absorbed in this material, resulting in more heating of the surrounding material and less energy impinging upon the corrosion thus less induced heating of the corrosion. For this simulation, orthogonal polarization was assumed (shown in Fig. 1 to be optimal for thin corrosion), with a corrosion thickness of 1 mm. Fig. 4a shows the temperature difference, as a function of loss tangent of concrete, between the maximum temperature on the surface of the concrete block located above the corroded rebar with respect to the temperature above the clean rebar. Upon considering these results, a few important points can be made. First, for low moisture conditions (represented above by a loss tangent of ~ 0.1 – 0.3), as the loss tangent increases, a decrease in temperature difference is evident. This indicates that even though the concrete absorbs more of the microwave energy, the presence of corrosion is still evident. However, for conditions of increased moisture presence (represented here by a loss tangent of 0.3 or greater) the temperature above the rebar exhibits very little change. This may be limiting with regards to detection of corroded rebar, but points to another potential application of this method, namely, detection of moisture ingress. The temperature sensitivity to the presence of corrosion may be improved by increasing the incident power (as only 10 W was considered here) or utilizing circular polarization.
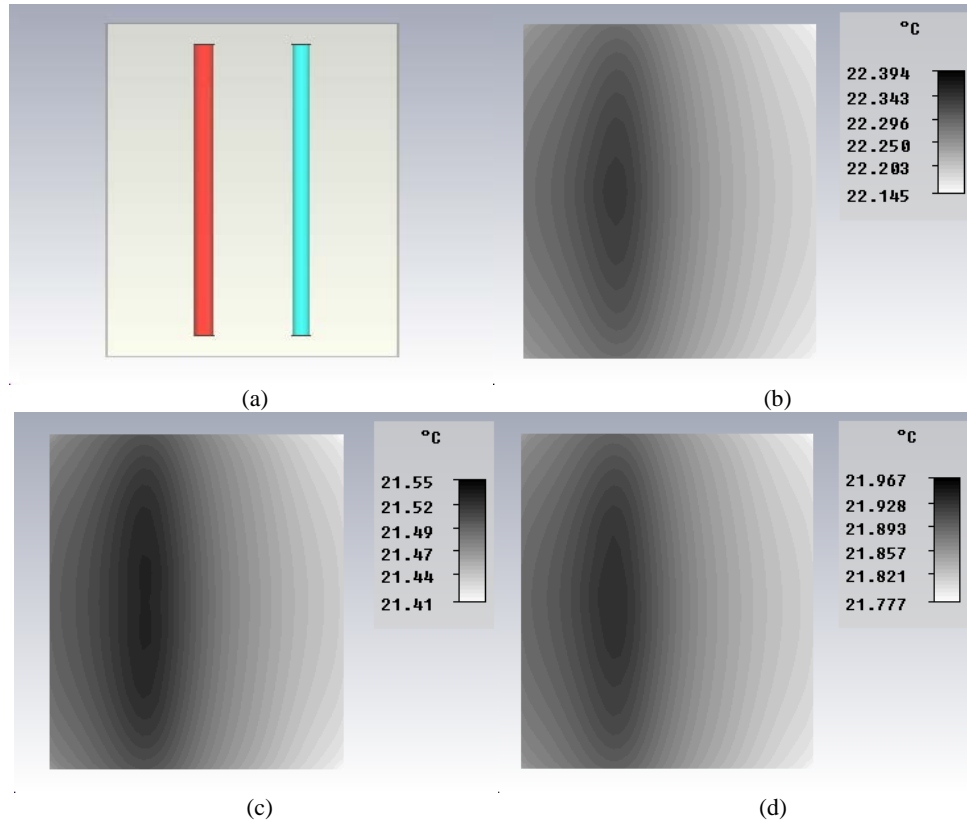
**FIGURE 3.** (a) Corroded (left) and non-corroded (right) rebar samples embedded in shallow concrete. Heat distribution caused by (b) orthogonal polarization, (c) parallel polarization, and (d) circular polarization.

Finally, simulations were conducted to investigate the effect of corrosion thickness on heating, with a fixed concrete loss tangent of 0.1. The maximum temperature on the surface of the concrete block (above the corroded rebar) as a function of corrosion thickness is shown in Fig. 4b. In this case and as expected, the temperature increases proportionally to corrosion thickness.
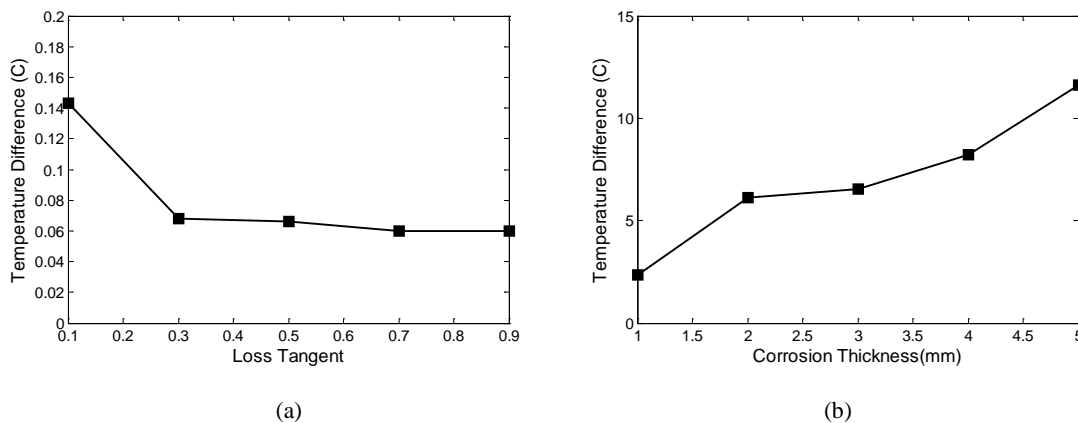


**FIGURE 4.** Maximum surface temperature as a function of (a) loss tangent of concrete, and (b) corrosion thickness.

# MEASUREMENTS

The simulations presented above indicate AMT has significant potential as a nondestructive testing tool for the infrastructure industry. To this end and to lend further credence to this new proposed technique, measurements were conducted on clean and corroded rebar in air and embedded in a concrete block. For these preliminary proof-of-concept measurements, a commercial countertop microwave oven was used as the source of the microwave energy. As such, direct comparison to the simulated results above is not possible, as the signal within a microwave oven consists of many modes/polarizations.

## Rebar in Air

To begin, two rebar samples were obtained; one with light corrosion (on the order 0.2 mm or less) along half of its length, the other with localized significant corrosion (on the order of 1-4 mm) on a portion of its length. These rebar samples are shown below in Fig. 5a. Each of these samples was exposed to microwave energy for 5 sec, and immediately following, imaged using a thermal camera (FLIR Thermacam SC 500), shown below in Fig. b-c (corroded area indicated in the black oval). It should be noted that the samples were placed on a plastic platform for testing, which is evident in the images below.

As can be seen in Fig. 5b-c, for both light and significant corrosion, the corrosion exhibited increased heating as opposed to the clean rebar. For the case of the lightly-corroded rebar, the temperature increase was nearly 600° mC (well above the sensitivity of the FLIR thermal camera, 100° mC). In addition and as expected, more heat was generated in the localized significant corrosion (nearly 3000° mC), as compared to the light corrosion. While these results are quite encouraging, it is also important to more accurately replicate what may be found in practice. To this end, a concrete sample with clean and corroded rebar was cast, and measurements were performed using this sample as well.

## Rebar Embedded in Cement

As shown below in Fig. 6, a concrete sample (dimensions of 17 cm × 15 cm × 5 cm) containing two rebars (one clean and one highly corroded) was cast using Quikcrete™ brand concrete mix. The rebars were embedded ~2.5 cm in the concrete. After 24 hours, the sample was demolded and placed in an oven (for ~1 week) at a temperature of 38° C to remove additional water in the sample. After removing the sample from the oven and allowing it to return to ambient temperature, the sample was exposed to 15 sec of microwave energy. Then, using the same thermal camera as above , an image was captured of the sample (see Fig. 6). Clearly (and as indicated by the black oval), the corroded rebar is detectable in the thermal image after microwave heating. The clean rebar is also evident in the image as well (left of the black oval), appearing as a lower-temperature line. Uneven heating is also evident in the sample, potentially due to the distribution of the microwave energy in the commercial microwave oven.



(a)  (b)  (c)
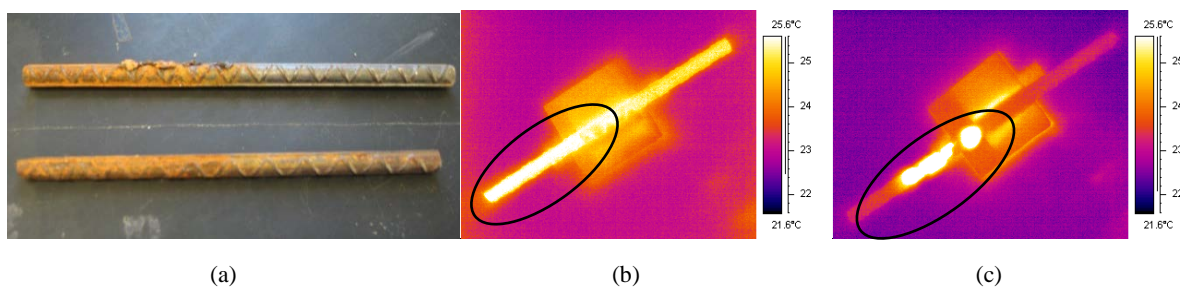
**FIGURE 5.** (a) Rebar with localized significant (top), and light corrosion (bottom). Thermal image of rebar with (b) light corrosion, and (c) localized corrosion.
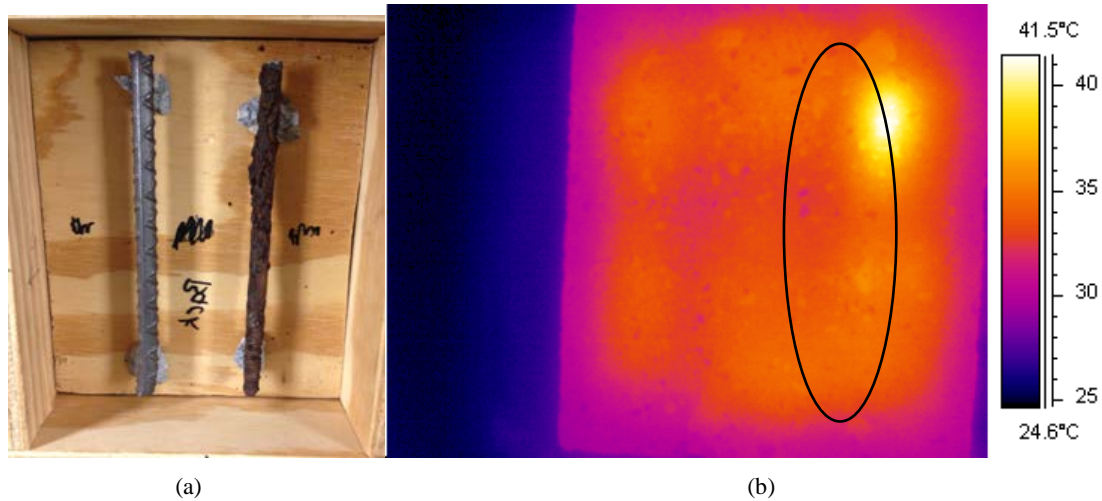
**FIGURE 6.** Photograph of clean (left) and corroded (right) rebar, and (b) thermal image of concrete block surface after microwave heating (location of corroded rebar indicated in the black oval).

# CONCLUSION

This paper presented preliminary simulation and measurement results on the use of active microwave heating and thermography for the detection of corrosion on rebars in concrete structures. These results showed that the increased absorption of the microwave energy by corrosion leads to a measureable increase in the surface temperature of the surrounding concrete. The simulations showed that the polarization of the incident signal can be optimized per the orientation and thickness of corrosion. Further, circular polarization was shown to perform better if prior knowledge of corrosion thickness and/or rebar orientation is not known. In addition, the presence of moisture and/or chloride ingress in concrete will lead to a higher loss tangent (and also may change the thermal properties) and therefore may also be detected using this technique. Future work may involve optimizing the required power and frequency of operation as well as utilizing more advanced measurement techniques such as pulsed microwave excitation and synchronized thermal detection. Further study on the effect of polarization for specific geometries/application may provide additional insight for optimizing this method. Specialized antenna design may also be beneficial in order to locally heat an area of interest, as opposed to applying microwave energy to an entire structure.

# ACKNOWLEDGEMENT

# REFERENCES

1. Koch, G. H., Brongers, M. P. H., Thompson, N. G., Virmani, Y. P., & Payer, J. H., "Corrosion costs and preventive strategies in the United States. Report by CC Technologies Laboratories, Inc. to Federal Highway Administration (FHWA)", Office of Infrastructure Research and Development. Report FHWA-RD-01-156, 2001.
2. Poursaee, A., "Corrosion Measurement Techniques in Steel Reinforced Concrete", *Journal of ASTM Intern., 8*, 1-15, 2011.
3. Ervin, B., Kuchma, D., Bernhard, J., and Reis, H., "Monitoring Corrosion of Rebar Embedded in Mortar Using High-Frequency Guided Ultrasonic Waves." *J. Eng. Mech.*, 135(1), 9–19, 2009.
4. Arndt, R. and F. Jalinoos, "NDE for corrosion detection in reinforced concrete structures: A benchmark approach", *Proceedings of Non-destructive Testing in Civil Engineering*, Nantes, France, June 30- July 3, 2009.
5. Jönsson, M., B. Rendahl, and I. Annergren, "The use of infrared thermography in the corrosion science area", *Materials and Corrosion, v*ol. 61, no. 11, 961-965, November 2010.
6. Kharkovsky, S., J.T. Case, M.T. Ghasr, R. Zoughi, S.W. Bae, and A. Belarbi "Application of Microwave 3D Imaging Techniques for Evaluation of Corrosion in Steel Rebars Embedded in Cement-Based Structures," *in Review of Progress in*

*Quantitative Nondestructive Evaluation Vol. 31B,* Burlington, VT, July 17-22, vol. 1430, AIP Conference Proceedings, edited by D.O. Thompson and D.E. Chimenti, American Institute of Physics, pp. 1516-1523, Melville, NY, 2011.

7.  Lesniak, J.R., and B.R. Boyce, "Differential Thermography Applied to Structural Integrity Assessment", *SPIE Thermosense XVII: An International Conference on Thermal Sensing and Imaging Diagnostic Applications*, vol. 2473, 179, March 1995.

8.  K.E. Cramer and Winfree, W.P., "Thermographic Imaging of Cracks in Thin Metal Sheets", *SPIE Thermosense XIV*, vol. 1682, 162-170, 1992.

9.  Mian, A., X. Han, M. Islam, and G. Newaz, "Fatigue damage detection in Graphite/Epoxy composites using sonic infrared imaging technique", *Journal of Composites Science and Technology*, vol. 64/5, 657-666, April 2004.

10. Baek, S., W. Xue, M.Q. Feng, and A. Kwon, "Nondestructive Corrosion Detection in RC Through Integrated Heat Induction and IR Thermography", *Journal of Nondestructive Evaluation*, vol. 31, 181-190, 2012.

11. K.J. Bois, Benally, A.D.; Nowak, P.S.; Zoughi, R., "Cure-state monitoring and water-to-cement ratio determination of fresh Portland cement-based materials using near-field microwave techniques," *IEEE Transactions on Instrumentation and Measurement*, vol. 47, no. 3, 628-637, June 1998.

12. K.J. Bois, Benally, A.D.; Zoughi, R., "Microwave near-field reflection property analysis of concrete for material content determination," *IEEE Transactions on Instrumentation and Measurement*, vol. 49, no. 1, 49-55, February 2000.

13. Bois, K., A.D. Benally, P.S. Nowak and R. Zoughi, "Application of near-Field microwave sensing techniques for aggregate segregation detection in concrete members," *Proceedings of the Twenty-sixth Annual Review of Progress in Quantitative Nondestructive Evaluation*, vol. 19B, 1717-1722, Montreal, Quebec, Canada, July 25-30, 1999.

14. S. Peer, Case, J.T.; Gallaher, E.; Kurtis, K.E.; Zoughi, R., "Microwave reflection and dielectric properties of mortar subjected to compression force and cyclically exposed to water and sodium chloride solution," *IEEE Transactions on Instrumentation and Measurement*, ,vol. 52, no. 1, 111-118, February 2003.

15. S. Peer, Zoughi, R., "Comparison of water and saltwater movement in mortar based on a semi empirical electromagnetic model," *Proc. of the 20th IEEE Instrumentation and Measurement Technology Conference*, vol. 1, 513-517, May 2003.

16. Sakagami, T., S. Kubo, T. Komiyama, and H. Suzuki, "Proposal of a New Thermographical Nondestructive Testing Technique Using Microwave Heating", *SPIE Conference on Thermosense XXI*, vol. 3700, 99-103, 1999.

17. Qaddoumi, N., L. Handjojo, T. Bigelow, J. Easter, A. Bray and R. Zoughi, "Microwave Corrosion Detection Using Open-Ended Rectangular Waveguide Sensors," *Materials Evaluation*, vol. 58, no. 2, 178-184, February 2000.

18. Laaidi, N., Belattar, S., Elbaloutti, A., "Thermal and Thermographical Modeling of the Rust Effect in Oil Conduits", *10th European Conference on Non-Destructive Testing*, June 2010

19. http://www.wolframalpha.com/input/?i=iron%28III%29+oxide&lk=1&a=ClashPrefs_*Chemical.IronIIIOxide-    (accessed 8/26/13).